CARBON letters

Note

Carbon Letters Vol. 25, 117-121 (2018)

Hierarchical porous carbon materials with ultrahigh specific surface area prepared from coal for supercapacitors

Peng Chang and Zhihong Qin*

School of Chemical Engineering and Technology, China University of Mining and Technology, Xuzhou 221116, China

Article Info

Received 9 August 2017
Accepted 10 October 2017

***Corresponding Author**
E-mail: qinzh1210@163.com

Open Access

DOI: http://dx.doi.org/10.5714/CL.2018.25.117

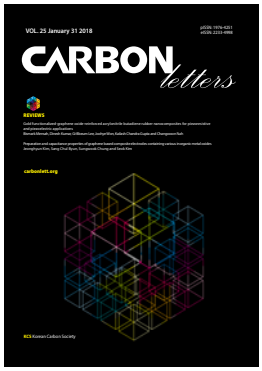

http://carbonlett.org

pISSN: 1976-4251
eISSN: 2233-4998

Supercapacitors are an excellent alternative to traditional methods of energy storage like batteries and dielectric capacitors, meanwhile coal as the most affordable and abundant energy resource currently, has also been commonly used as carbon source for electrode materials of supercapacitors [1-4]. Considering the sustainable development of resource and environment protection, how to realize the utilization of coal with high ash matter cleanly and effectively, has become an important issue to researchers. Compared with the complicated, time-consuming and high cost traditional demineralization method, we creatively introduce extraction and back-extraction method to obtain the desired ash-free group component-loose medium component (LMC) from raw coal and adopt it as the precursor for preparation of hierarchical porous carbon materials (HPCs) [5,6].

HPCs have been extensively studied as a promising electrode candidate for supercapacitors because of their large specific surface area (SSA), ideal hierarchical porous structure and low cost [7]. Generally, the capacitive capability of supercapacitors highly depends on the electrode materials. Hence, tailoring the porous structure of carbon materials is of great importance in enhancing their electrochemical performance [8]. The SSAs of materials activated by $ZnCl_2$ are relatively low, while KOH as a commonly used activation agent can be adopted as reactivation agent to efficiently develop a large number of micropores and obtain a better porous structure [9]. Thus, herein, we report a two-step activation strategy using $ZnCl_2$ and KOH as activators to prepare HPCs with ultrahigh SSA from LMC.

Huaibei fat coal with 24.2% of ash content was used in this study. The proximate and ultimate analyses of raw coal and LMC are listed in Table 1. As we can see, after the extraction and back-extraction process, ash content of LMC decreases to 2%. Extensive experimental details of extraction and back-extraction method have been published in our previous works [6].

For a typical run, $ZnCl_2$ and LMC were ground and mixed in mortar with a mass ratio of 2:1. The resultant mixture was heated to 500°C at 5°C/min and kept for 1 h under flowing nitrogen in a tube furnace. The activated product was washed repeatedly with 2 M HCl and distilled water until the pH value of filtrate reached 7. After drying, the final product and KOH (mass ratio 1:6) were thoroughly mixed and then activated at 750°C for 1 h with a heating rate of 5°C/min. Finally, the obtained sample was denoted as HPC-1, where 1 represents first-step activation time. For comparison, other two samples were prepared at the first-step activation time of 0 h and 2 h respectively.

The morphology of HPCs was analyzed by transmission electron microscopy (TEM, FEI Tecnai G^2 F20) and scanning electron microscopy (SEM, FEI Quanta TM 250). Pore structure of the samples was characterized by N_2 adsorption/desorption isotherms at 77 K with an Autosorb-1-MP analyzer (Quantachrome).

The working electrode was prepared by mixing 85 wt% of HPCs, 10 wt% of acetylene black, and 5 wt% of PTFE glue, then coated onto nickel foam at 5 MPa. All electrochemical tests were performed in a 6 M KOH electrolyte using two-electrode system on Ivium Vertex electrochemical workstation with a potential window of 0–1 V.

From the SEM images of HPCs in Fig. 1a-c, we can find that under the same magnification, the HPCs with different first-step activation time possess completely different morphologies. In Fig. 1a, HPC-0 shows a large block structure with rugged surface and little macropores on the outside surface due to the insufficient activation reaction process. As provided

Table 1. Proximate and ultimate analyses of raw coal and LMC

Sample	Proximate analysis (wt%)				Ultimate analysis (wt%)				
	M_{ad}	A_d	V_{daf}	FC_{daf}	C_{daf}	H_{daf}	O_{daf}[a)]	N_{daf}	$S_{t,daf}$
Raw coal	1.27	24.20	24.94	75.06	86.50	5.05	6.32	1.47	0.66
LMC	0.48	2.21	27.53	75.63	84.72	5.20	6.72	2.59	0.77

[a)]By difference.

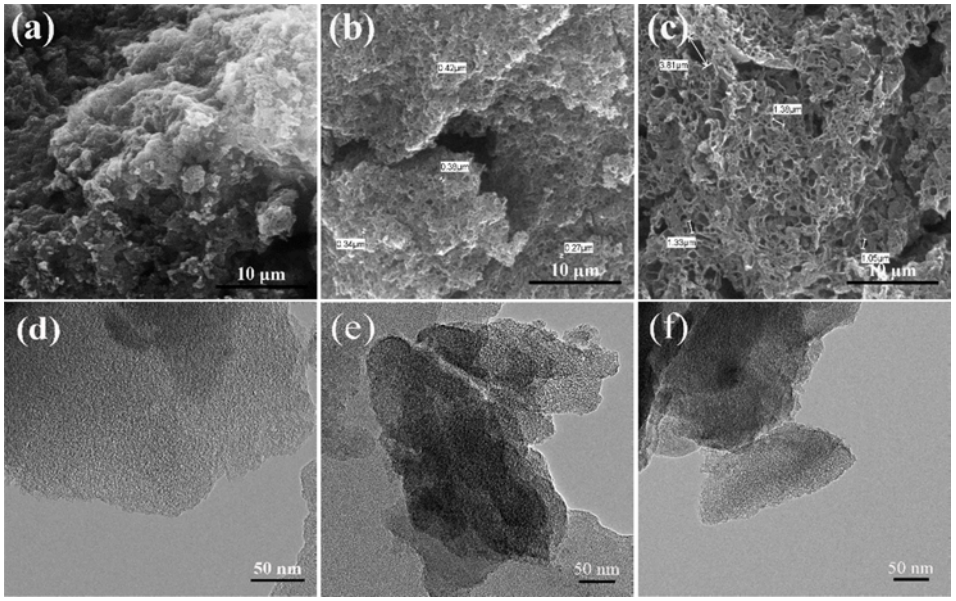

Fig. 1. SEM images of (a) HPC-0, (b) HPC-1, (c) HPC-2; TEM images of (d) HPC-0, (e) HPC-1, (f) HPC-2.

in Fig. 1b, HPC-1 displays a typical layered stacking structure with abundant macropores (200–500 nm) on the large sheets which could serve as ion-buffering reservoirs to efficiently shorten the ion transport distance. SEM image of HPC-2 in Fig. 1c demonstrates a disordered foam-like structure and the pore size is mostly in the range of 1–5 μm which may be induced by the overlong of activation time. It is noteworthy that the rise of first-step activation time from 0 h to 2 h results in tremendous changes of surface morphology and great increases in macropore porosity and pore diameter due to the pore widening effect of longer activation time.

Fig. 1d-f show the TEM images of HPCs. In the case of HPC-0, the TEM observation (Fig. 1d) reveals a typical microporous structure, in which many micropores can be clearly observed while barely mesopores can be observed, indicating that the short activation time is unfavorable to the formation of mesopores. In Fig. 1e, TEM image of HPC-1 presents a disordered turbostratic structure and developed worm-hole type porosity with abundant ordered micropores and slit small mesopores (about 5 nm in diameter), further proving the ideal hierarchical porous system of HPC-1 which is propitious to the effective ion adsorption, fast ion transport and always brings about high specific capacitance. Compared with HPC-1, HPC-2 (Fig. 1f) exhibits a significant decline of textural properties in both microporous and mesoporous range which demonstrates that prolonged first-step activation time may lead to the collapse of formed pore walls and hinder the KOH etching reaction during the second-step activation process. These results indicate that the changes as the first-step activation time gradually rises from 0 h to 2 h give rise to the variations in porous structure of HPCs, and in particular a fluctuation in the porosity in the small mesopore range.

Due to the Lewis acid nature, under high temperature conditions, $ZnCl_2$ serves the functions of catalytic dehydroxylation and dehydration [10-12]. During the activation process, $ZnCl_2$ works as acceptor center of electron pair to react with –OH in LMC, leading to the removing of hydrogen and oxygen atoms in the form of vapor. In the meantime, it also inhibits the formation of tars and any other liquids that may clog up the pores of the sample, and volatiles will be subsequently released from the carbon surface to develop a relatively well-developed micro- and mesoporous structure [13,14]. While the prominent reaction occurring between KOH and carbon materials is mostly as follows: $6KOH+2C \rightarrow 2K+3H_2+2K_2CO_3$ [15]. On the basis of existing pore structure created by $ZnCl_2$, more abundant micropores can be created by the reactivation of KOH. On the other hand, the existing microporous structure will be expanded by the pore-widening function of KOH etching reaction, so as to effectively increase the mesopore content and realize the effective construc-

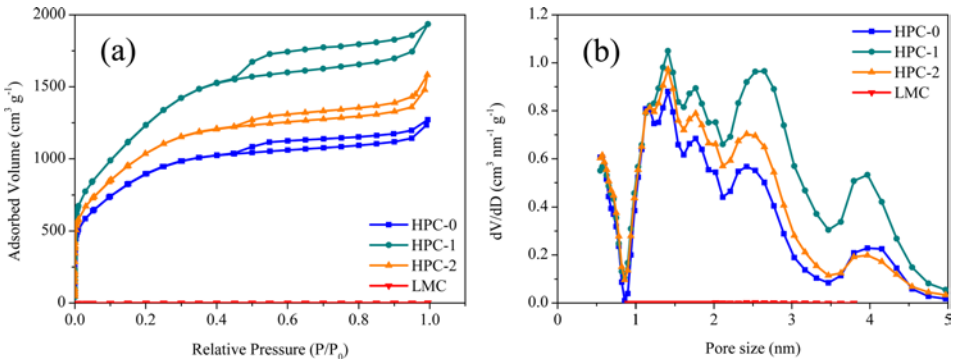

Fig. 2. (a) Nitrogen adsorption-desorption isotherms and (b) pore size distributions of LMC and HPCs.

Table 2. Textural characteristics of LMC and HPCs

Sample	S_{BET} (m^2 g^{-1})	V_t (cm^3 g^{-1})	V_{micro} (cm^3 g^{-1})	V_{meso} (cm^3 g^{-1})	D_{ap} (nm)
LMC	3	0.003	0.001	0.001	4.09
HPC-0	3276	1.76	1.28	0.44	2.16
HPC-1	4672	2.99	1.73	0.98	2.57
HPC-2	3877	2.05	1.47	0.51	2.12

tion of hierarchical porous structure.

To understand the influence of first-step activation time on the development of porous structure in HPCs, the samples were characterized by N_2 adsorption/desorption analyses. Fig. 2a shows the N_2 adsorption/desorption isotherms of LMC and HPCs. It can be clearly seen that the LMC without any activation process adsorbs less than 2 cm^3 g^{-1} of N_2 at 0.99 of the relative pressure (P/P_0, where P_0 is the saturation vapor pressure of N_2 at 77 K), while the adsorbed volumes of HPCs are all more than 1000 cm^3 g^{-1}, even reach to 2000 cm^3 g^{-1}, which are much higher than that of LMC, illustrating the developed porous structures of HPCs induced by the two-step activation process. According to the International Union of Pure and Applied Chemistry (IUPAC) classification, isotherms of HPCs all exhibit combined characteristics of type I and IV with a H4 type hysteresis loop. The strong N_2 uptake at P/P_0 <0.01 corresponds to the filling of abundant micropores, while the hysteresis loop at 0.4<P/P_0<1.0 assigns to the capillary condensation in mesopores. By comparison, HPC-1 possesses the largest hysteresis loop area and adsorbed volume, suggesting the existences of well-developed microporosity and a large number of mesopores which could facilitate rapider ion mobility.

The density functional theory pore size distributions in Fig. 2b show that along with the increasing of first-step activation time, the pore size distributions of HPCs change significantly. Yet, the pore size distributions of HPCs are relatively narrower and only a tiny fraction of mesopores appear when the first-step activation time exceeds or falls short of 1 h. Compared with other HPCs, there are more small mesopores coexist with more abundant micropores in HPC-1, which are beneficial to the fast diffusion of ions in electrolyte and always lead to a promising electrochemical performance.

Table 2 summarizes the textural properties of LMC and HPCs. As we can see, LMC possesses very low surface area (3 m^2 g^{-1}) because of its nonporous characteristics, as proved by the extremely low N_2 adsorption capacity. However, it is clear that both the surface area and pore volume of LMC sharply increase through two-step activation process. As shown in Table 2, HPC-1 exhibits an incredibly high SSA of 4672 m^2 g^{-1}, with V_t of 2.99 cm^3 g^{-1} and V_{meso}/V_{micro} value of 0.57, implying an unique hierarchical porous structure with extremely developed microporous structure and ideal ratio of micro/mesopores which is also in well accordance with the TEM image in Fig. 1e. When first-step activation time is 1 h, micropores generated on layered structure are easily further activated to form mesopores by pore widening and fusing during the KOH etching process. While both further increase or decrease of activation time would remarkably reduce SSA, V_t, and V_{meso} due to the incomplete activation process or micropores collapsing caused by over-activation.

Fig. 3a displays the cyclic voltammograms (CV) curves of HPCs with quasi-rectangular shape collected at 10 mV s^{-1}. Meanwhile, it can be clearly seen that the CV curve of HPC-1 exhibits the largest integral loop area and the slightest deviation from rectangular shape, implying the greatest accessibility of electrolyte ions into electrode surface and the highest specific capacitance at relatively low scan rate. Furthermore, the current response of HPC-0 is smaller than that of HPC-2, that is to say, the specific capacitance of HPC-0 is the lowest among all samples studied which is also in accordance with the measurement results of porous structure.

Galvanostatic charge-discharge (GCD) curves of HPCs at 1 A g^{-1} are shown in Fig. 3b. The GCD curves of samples demonstrate symmetrical and linear profiles, which are the typical characteristics of ideal supercapacitors. A dramatically falling region can be observed in the discharging region. This is known as the current resistance (IR) drop and is caused by the internal

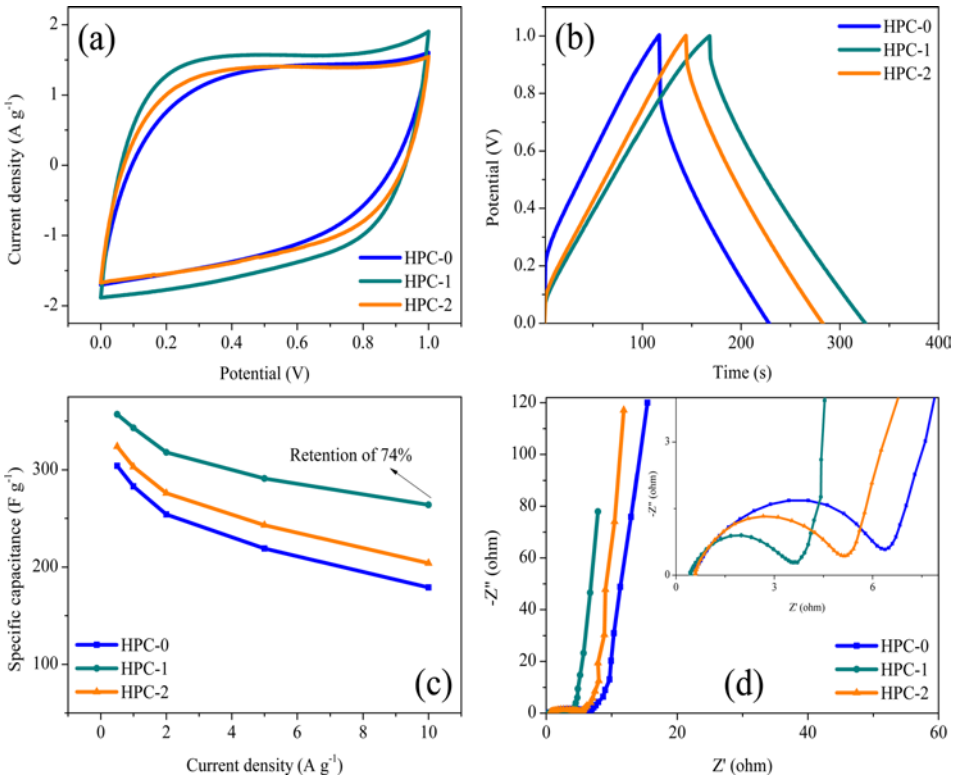

Fig. 3. (a) CV curves at 10 mV s^{-1}, (b) GCD curves at 1 A g^{-1}, (c) rate performance, and (d) electrochemical impedance spectra of HPCs.

resistance of the electrode materials. The IR drops in the 1 A g^{-1} discharge profiles are 0.215, 0.069, and 0.108 V respectively at first-step activation time of 0, 1, and 2 h, which are corresponding with the textural properties of HPCs, indicating that the excessive or insufficient activation process are responsible for higher internal resistance in this kind of supercapacitors. Specially, HPC-1 presents the longest discharge time and the smallest IR drop, signifying the most excellent supercapacitive behavior and the greatest pore accessibility for electrolyte. While the very low specific capacitance and the largest IR drop found for HPC-0 agree with the presence of less mesopores and macropores, which is caused by an incomplete activation process, as already discussed. The reasonable meso-/macropores could serve as favorable paths and electrolyte reservoirs to realize fast ion transportation and obtain a high diffusion efficiency during the ions adsorption process.

Fig. 3c shows the rate abilities of HPC electrodes at different discharge rates from 0.5 to 10 A g^{-1}. It can be clearly observed that the capacitance retention of samples decreases in the order of HPC-1 (74%) > HPC-2 (63%) > HPC-0 (58%), demonstrating that relatively more mesopores and macropores can result in a better capacitance retention, which is in agreement with Fig. 3b. Furthermore, the specific capacitance of HPC-1 is always higher than that of other samples at the same current density. It should also be noted that, the capacitance value of HPC-1 reaches 357 F g^{-1} at 0.5 A g^{-1} and retains 264 F g^{-1} at 10 A g^{-1}. The outstanding rate capability and great capacitance performance are ascribed to that the HPC-1 electrode possesses ultrahigh SSA and ideal hierarchical pore system which could function as active sites and expressways for ion adsorption and fast ion diffusion. On the contrary, to HPC-0, too few macropores and high ratio of V_{micro} to V_{meso} directly lead to the worst rate performance.

As illustrated in Fig. 3d, the electrochemical impedance spectra of samples show that the intersecting points on the real axis at high frequency which represent for the bulk resistance (R_s) are almost identical. However, the charge transfer resistances (R_{ct}) of HPCs derived from the semi-circles in the high-medium frequency range are significantly different, exhibiting a sharply raise with the increase or decrease of first-step activation time from 1 h. It means that the electrodes with excessive or insufficient first-step activation process (HPC-2, HPC-0) have higher R_{ct}. At a very low frequency, an ideal capacitance would give rise to a straight line parallel to the imaginary axis. The more inclined the line is, the more diffusion resistive element exists. These results demonstrate that the HPC-1 electrode exhibits the lowest R_{ct} and diffusion resistance, and thus the lowest internal resistance, which is also consistent with the above analysis results.

The charge/discharge cycling test at a current density of 5 A g^{-1} of HPC-1 electrode displayed a good cyclic stability (Fig. 4). It can be seen that HPC-1 renders a high capacity retention of about 95% after 5000 charge-discharge cycles at 5 A g^{-1}. Such excellent cycling performance should be attributed to its unique hierarchical porous structure which is helpful for both good electron conduction and fast ion transport.

In summary, HPCs with ultrahigh SSA of 4672 m^2 g^{-1} and remarkable pore volume of 2.99 cm^3 g^{-1} were effectively prepared from LMC by two-step activation method. The results of this study showed that LMC used is a good candidate for HPCs production and the surface characteristics of HPCs change signifi-

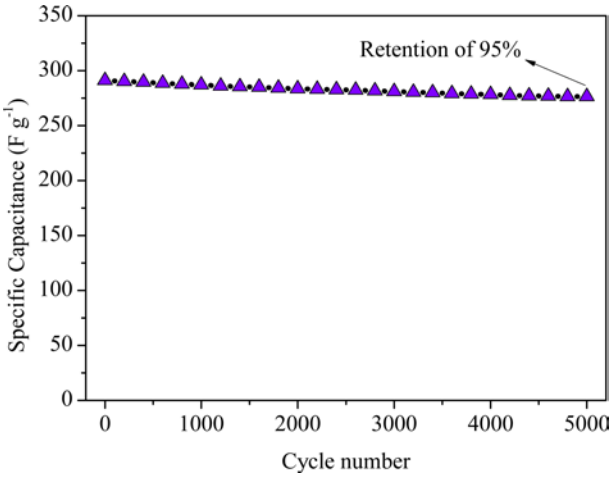

Fig. 4. Cycle stability of HPC-1 measured at 5 A g^{-1}.

cantly with first-step activation time. The specific capacitance of HPC-1 reaches 357 F g^{-1} at 0.5 A g^{-1} with about 74% capacitance retention at 10 A g^{-1}. Furthermore, the HPC-1 maintains a high capacitance remaining capability of 95% after 5000 cycles at a current density of 5 A g^{-1}, indicating a promising electrode material for supercapacitor. In addition, the prepared novel HPCs also present great potential as an excellent absorbent material to be used in the fields of gas storage, catalyst supports, and electrode materials.

Conflict of Interest

No potential conflict of interest relevant to this article was reported.

Acknowledgements

This work was supported by National Natural Science Foundation of China (51674260, 51274201).

References

[1] Simon P, Gogotsi Y. Materials for electrochemical capacitors. Nat Mater, **7**, 845 (2008). https://doi.org/10.1038/nmat2297.

[2] Zhao Z, Xie Y. Enhanced electrochemical performance of carbon quantum dots-polyaniline hybrid. J Power Sources, **337**, 54 (2017). https://doi.org/10.1016/j.jpowsour.2016.10.110.

[3] Wang LP, Zhou Y, Qiu JS. Title. Micropor Mesopor Mat, **3**, 67 (2013). DOI .

[4] Frackowiak E. Carbon materials for supercapacitor application. Phys Chem Chem Phys, **9**, 1774 (2007). https://doi.org/10.1039/b618139m.

[5] Huang G, Kang W, Xing B, Chen L, Zhang C. Oxygen-rich and hierarchical porous carbons prepared from coal based humic acid for supercapacitor electrodes. Fuel Process Technol, **142**, 1 (2016). https://doi.org/10.1016/j.fuproc.2015.09.025.

[6] Chang P, Qin Z. Facile fabrication of hierarchical porous carbon based on extract separated from coal with outstanding electrochemical performance. RSC Adv, **54**, 33843 (2017). https://doi.org/10.1039/c7ra05437h.

[7] Luan Y, Xue YW, Shi ZG. Synthesis of hierarchically macro/meso/microporous carbon spheres and its application in fast rechargeable electric double layer capacitor. Mater Lett, **88**, 30 (2012). https://doi.org/10.1016/j.matlet.2012.08.046.

[8] Liu C, Li F, Ma LP, Cheng HM. Advanced materials for energy storage. Adv Mater, **22**, E28 (2010). https://doi.org/10.1002/adma.200903328.

[9] Zhang J, Zhang W. Preparation and characterization of activated carbon fibers from liquefied poplar bark. Mater Lett, **112**, 26 (2013). https://doi.org/10.1016/j.matlet.2013.08.103.

[10] Ahmadpour A, Do DD. The preparation of activated carbon from macadamia nutshell by chemical activation. Carbon, **35**, 1723 (1997). https://doi.org/10.1016/s0008-6223(97)00127-9.

[11] Ahmadpour A, Do DD. The preparation of active carbons from coal by chemical and physical activation. Carbon, **34**, 471 (1996). https://doi.org/10.1016/0008-6223(95)00204-9.

[12] Lua AC, Yang T. Characteristics of activated carbon prepared from pistachio-nut shell by zinc chloride activation under nitrogen and vacuum conditions. J Colloid Interface Sci, **290**, 505 (2005). https://doi.org/10.1016/j.jcis.2005.04.063.

[13] Xiang X, Liu E, Huang Z, Shen H, Tian Y, Xiao C, Yang J, Mao Z. Preparation of activated carbon from polyaniline by zinc chloride activation as supercapacitor electrodes. J Solid State Electrochem, **15**, 2667 (2011). https://doi.org/10.1007/s10008-010-1258-7.

[14] Rufford TE, Hulicova-Jurcakova D, Khosla K, Zhu Z, Lu GQ. Microstructure and electrochemical double-layer capacitance of carbon electrodes prepared by zinc chloride activation of sugar cane bagasse. J Power Sources, **195**, 912 (2010). https://doi.org/10.1016/j.jpowsour.2009.08.048.

[15] Wang L, Wang R, Zhao H, Liu L, Jia D. High rate performance porous carbon prepared from coal for supercapacitors. Mater Lett, **149**, 85 (2015). https://doi.org/10.1016/j.matlet.2014.11.051.